Wide-band B-spline wavelet with four parameters

Siyuan Cao*, CNPC Key Laboratory of geophysical, China University of petroleum
De-hua Han, University of Houston

Summary

Based on the wavelet decomposition theory of seismic pulse and its reconstruction, we proposed one method to make of wide-band wavelet. A series of seismic wavelets can be made in this way. In virtue of complex frequency B-spline wavelet, we formed the wide-band B-spline wavelet with four parameters and deduced its analytic expression both in the time domain and in the frequency domain. The numbers and energy of side lobes of the new wide-band B-spline wavelet with four parameters can be easily adjusted through its parameters. In comparison with the Ricker wavelet and wide-band Ricker wavelet in the condition of same main lobe equivalent frequency, the wide-band B-spline wavelet with four parameters not only has smaller side lobe but also has shorter time length. The synthetic result of wedge model indicated that the wide-band b-spline wavelet with four parameters has higher resolution. Finally, we also discussed its parameters adjustment in the practical application. Therefore, the seismic data processors and interpreters may have more seismic wavelet selections conveniently.

Introduction

Reflection seismic signal can be viewed as low pass filtered reflectivity series, and the seismic amplitude varies with the change of impedance. The change of the seismic waveform is associated with the sedimentary and diagenesis history as well as the fore filled fluids; therefore the study of the seismic wavelet is an essential topic in exploration geophysics. It is commonly believed the dynamite source generates a spike pulse. And this spike pulse gradually transforms into a stable continuous multiple lobe waveform that is called wavelet. The resolution of the wavelet directly influences the resolution of seismic data. In seismic processing, we normally use a high resolution theoretical wavelet as the expected output of deconvolution, to improve the seismic data resolution. While traveling through the hydrocarbon saturated rocks, the seismic wavelet can has its energy dissipated with the high frequency part more attenuated. By studying the wavelet spectra variation, we can analyze the absorption character of the reservoir and estimate the hydrocarbon saturation. In forward modeling, wavelets are used with wave equations or models to generate synthetic seismic data. In reservoir inversion, the selection of the right wavelet and its scale is critical to the inversion result.

In practical applications, there are very limited theoretical wavelets available. Commonly used wavelets include Ricker wavelet and wide band Ricker wavelet. Ricker wavelet has large side lobes which contain 44.63% energy of the main lobe. Its main lobe is wide resulting low time resolution. Compared with Ricker wavelet, wide band wavelet has narrower main lobe, smaller side lobes and higher resolution. But its larger time length can be truncated by narrow time window in real processing practice. In this paper, we propose a new set of theoretical wavelet that has higher time resolution compared with other wavelets with the same main lobe equivalent frequency.

Wavelet decomposition and reconstruction on seismic impulse

Grossmann and Morlet (1984) defined the continuous wavelet transform. A function $\varphi(x) \in L^2(R)$ is called a wavelet function if it averages to 0 and satisfies the admissibility condition. By stretching or shrinking the scale s, and shifting the time u, we can obtain the wavelet base in (1):

$$\varphi_{u,s}(t) = \frac{1}{\sqrt{s}} \varphi\left(\frac{t-u}{s}\right) \tag{1}$$

After selecting wavelet function, the corresponding continuous wavelet transform can be thought as a cross correlation between the signal and the wavelet function after stretching/shrinking and shift.

$$Wf(u,s) = \frac{1}{\sqrt{s}} \int_{-\infty}^{+\infty} f(t)\varphi^*\left(\frac{t-u}{s}\right) dt = f * \overline{\varphi}_s(u) \tag{2}$$

here $\overline{\varphi}_s(t) = \frac{1}{\sqrt{s}} \varphi^*\left(-\frac{t}{s}\right)$, and $*$ represents complex conjugate.

The corresponding reverse continuous wavelet transform is called full scale signal reconstruction

$$f(t) = \frac{1}{C_\varphi} \int_{-\infty}^{+\infty} \int_{-\infty}^{+\infty} Wf(u,s)\varphi_{u,s}(t)/s^2 duds \tag{3}$$

here $1/C_\phi$ is a constant related to the selected wavelet.

A seismic impulse signal is characterized as a unit impulse with value 1 at time 0 and value 0 at all other time. Apply (2) to this signal, we can get wavelet decomposition of this impulse at different scales. If an orthogonal wavelet base is used, there is no redundancy in decomposition then the original signal can be uniquely recovered with full scale

reconstruction using (3). The scale of the decomposed wavelet is a representation of its main frequency. Using partial scale reconstruction, we can obtain a theoretical wavelet with demanded frequency band, as in (4):

$$f(t) = \frac{1}{C_\varphi} \int_p^q \int_{-\infty}^{+\infty} Wf(u,s) \varphi_{u,s}(t) / s^2 \, du \, ds$$

(4)

here p and q are up and low integral limits for scale s.

In Figure 1, we select the second derivative of Gaussian function as the wavelet mother function to decompose the seismic impulse, and then apply the partial scale reconstruction to obtain theoretical wavelet with high, median, and low frequency. The center red line is the original seismic impulse, while the blue, green, and red are partial scale reconstructed wavelet with scales 1-10, 11-20, and 21-30 respectively.
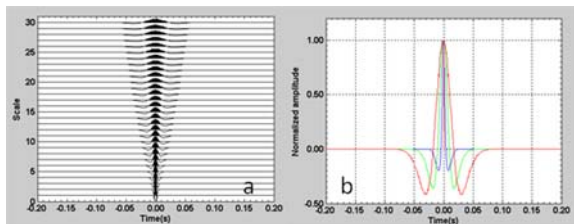

Figure1: Gauss 2 wavelet decomposition of seismic pulse (a) and its reconstruction (b).

The build of four parameter wide band B-spline wavelet

From the decomposition and reconstruction of seismic impulse theory, we can chose different mother wavelet to reconstruct different serious of partial scale wavelet base, each with its own unique features. Here we use B-spline complex wavelet as the mother wavelet. It satisfies the admissibility condition.

$$\varphi(t) = \sqrt{f_b} \left(\sin c \left(\frac{f_b t}{m} \right) \right)^m e^{i 2\pi f_c t}$$

(5)

here m is a integer, f_b represents band width, and f_c is the main frequency.

Use this mother wavelet to decompose the unit impulse, then reconstruct in the range [p,q], take the real part and simplify the result to obtain the wide band B-spline wavelet:

$$y(t) = \frac{1}{q-p} \sqrt{f_b} \left(\sin c \left(\frac{f_b t}{m} \right) \right)^m \left(q \sin c(2qt) - p \sin c(2pt) \right)$$

(6)

It contains four parameters m, f_b , p and q, thus is named four parameter wide band B-spline wavelet.

The properties and resolution of four parameter wide band B-spline wavelet

Apply the Fourier transform to (6), we obtain the amplitude spectrum of the four parameter wide band B-spline wavelet, as the convolution of multiple rectangular functions:

$$Y(f) = \frac{\sqrt{f_b}}{2(q-p)} \left(\frac{m}{2\pi f_b} \right)^m \left(\overbrace{rect\left(\frac{mf}{f_b}\right) * ... * rect\left(\frac{mf}{f_b}\right)}^{m} * \left(rect\left(\frac{f}{2q}\right) - rect\left(\frac{f}{2p}\right) \right) \right)$$

(7)

Figure 2(a) and 2(b) display the waveform and amplitude spectrum of a four parameter wide band B-spline wavelet, with m=5 and f_b=200, p and q to be 5Hz and 55Hz respectively.
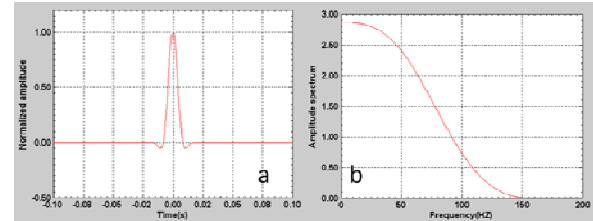

Figure2: Wave form of wide-band B-spline wavelet with four parameters (a) and its amplitude spectrum (b).

With simple manipulation, it is easy to derive that the maximum of (6) appears at t=0, and its maximum value $y(0) = \sqrt{f_b}$ is independent to the selection of low and up limit of reconstruction. The first positive zero-cross time is the minimum one among $t_{c1} = \frac{m}{f_b}$, $t_{c2} = \frac{1}{2(q+p)}$, $t_{c3} = \frac{1}{q-p}$. Its main lobe width is $2t_c$, normally with $t_{c2} < t_{c1}$ and $t_{c2} < t_{c3}$, unless when the side lobes attenuation approaches the limits, that is m sufficiently small, and f_b sufficiently large, the main lobe width approaches $2t_{c2}$. The equivalent frequency of the main lobe takes the maximum value among $f_{a1} = \frac{1}{4t_{c1}} = \frac{f_b}{4m}$, $f_{a2} = \frac{1}{4t_{c2}} = \frac{q+p}{2}$, $f_{a3} = \frac{1}{4t_{c3}} = \frac{q-p}{4}$.

To analyze their resolutions, in Figure 3 we compare the Riker wavelet (blue), wide band Ricker wavelet (green), and four parameter wide band B-spline wavelet (red) with same equivalent frequency in different aspects. The waveforms in Figure 3(a) show that four parameter wide band B-spline wavelet has the smallest side lobes and shortest wavelet time length. The wide band Riker wavelet also has a smaller side lobe than Ricker wavelet but the much larger wavelet time length can be truncated by the relatively shorter time window in real processing. The amplitude spectra in Figure 3(b) show that four parameter wide band B-spline wavelet contains more low frequency energy and has its peak frequency lower than Ricker and wide band Ricker wavelet. In Figure 3(c), the four parameter wide band B-spline wavelet exhibits higher maximum instantaneous frequency than other two wavelets and suggest a higher time resolution. To illustrate this, we plot the wedge model synthetics with those 3 wavelets in Figure 3(d), (e), (f). Finally in 3(g), we plot the tuning curves and pick the maximum amplitudes for 3 wavelets.

Wide Band B-Spline Wavelet

The result shows the four parameter wide band B-spline wavelet has the highest resolution.
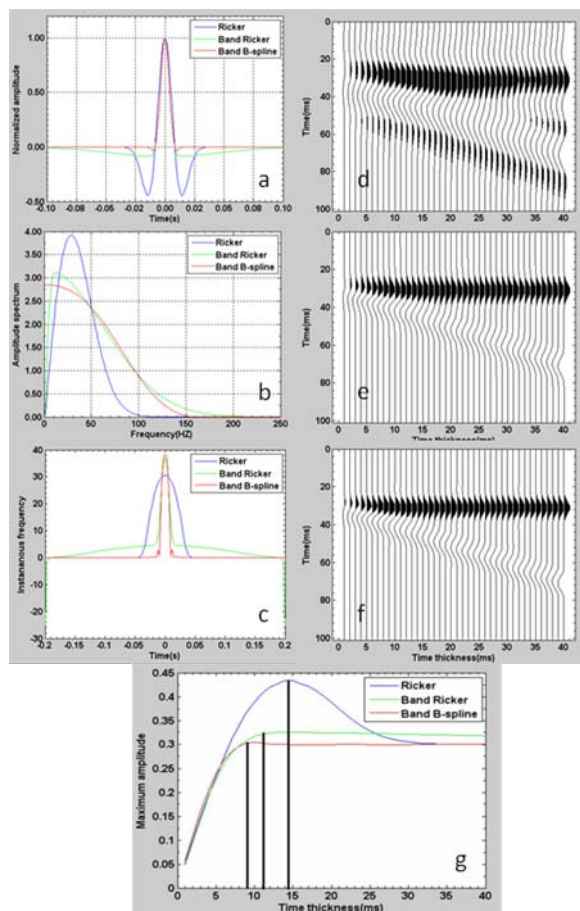

Figure3: Resolution comparison between wide-band B-spline wavelet with four parameters and Ricker, wide-band Ricker wavelet.

Parameter selection

From the time domain expression (6), four parameter wide band B-spline wavelet can be controlled by 4 parameters: order m, band width f_b, and frequency integral limit p and q. To provide a guide to real application, we discuss the influences of these 4 parameters on the waveform and spectrum. In Figure 4-7, (a) is wavelet waveform and (b) is corresponding amplitude spectrum.

Figure 4 demonstrates the effect of m. The color bar represents the increasing m value from 30 (blue) to 150 (red), with fixed f_b(200), p(5Hz) and q(20Hz). Parameter m controls the size of side lobes. By decreasing m, the side lobes are more attenuated. But for the main lobe, its maximum value and time width remain unchanged. The corresponding band pass property in 4(c) also is not changed.

Figure 5 demonstrates the effect of f_b. The color bar represents the increasing f_b value from 50 (blue) to 170 (red), with fixed m(40), p(5Hz) and q(20Hz). Parameter f_b controls the number of side lobes. By increasing f_b, the number of side lobes increases. For the main lobe, its maximum value increases but time width remains unchanged. The corresponding band pass property in 5(c) also is not changed.

Figure 6 demonstrates the effect of p. The color bar represents the increasing p value from 5Hz (blue) to 50Hz (red), with fixed m(10), f_b(250) and q(80Hz). Parameter p controls width of main lobe. By increasing p, the main lobe becomes narrower with unchanged maximum value. More side lobes appear with increasing size. In amplitude spectrum 6(c), increasing p mainly affects the left part of the spectrum, reduces the overall band width and move the center frequency to higher end.
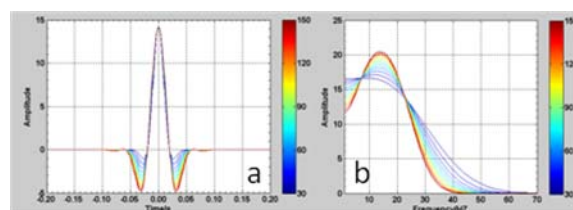

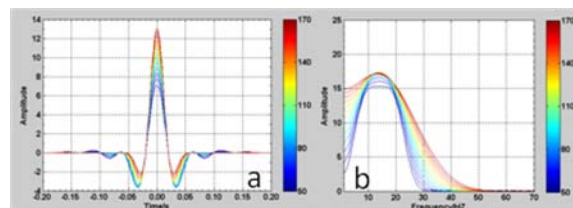Figure4: Parameter m selection of wide-band B-spline wavelet with four parameters

Figure5: Parameter f_b selection of wide-band B-spline wavelet with four parameters
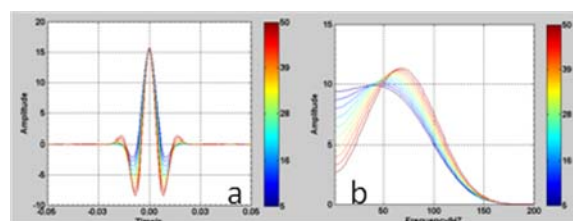

Figure6: Parameter p selection of wide-band B-spline wavelet with four parameters

Figure7: Parameter q selection of wide-band B-spline wavelet with four parameters

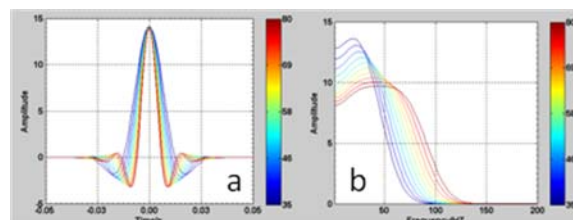Figure 7 demonstrates the effect of q. The color bar represents the increasing q value from 35Hz (blue) to 80Hz (red), with fixed m(10), f_b(250) and p(5Hz). Parameter q also controls width of main lobe. By increasing q, the main lobe becomes narrower with unchanged maximum value. More side lobes appear with increasing size. In amplitude spectrum 7(c), increasing q mainly affects the right part of the spectrum, increases the overall band width and move the center frequency to higher end.

The above tests demonstrate that four parameters can be used to flexibly adjust the waveform and spectrum of the wavelet. Parameter m and f_b control the energy and number of side lobes respectively. Integral limit parameters p and q control the main lobe width and band pass property. This is consistent with previous obtained main lobe expression t_{c2}. Increasing either p or q will reduce the main lobe width and increase both number and energy of the side lobes. To overcome this unexpected effect we can adjust the parameter m and f_b to reduce the number and energy of side lobes.

Conclusion

Based on the theory of wavelet decomposition and reconstruction on seismic impulse, a four parameter wide band B-spline wavelet is introduced. This wavelet has the advantages of small side lobe and shorter time length. Compared with Ricker and wide band Ricker wavelet with same equivalent frequency, this new wavelet has higher time resolution. The numbers and energy of side lobes of the new wide-band B-spline wavelet with four parameters can be easily adjusted through its parameters. It provides seismic processors and interpreters a new theoretical wavelet with more flexible selections and controls.

EDITED REFERENCES

Note: This reference list is a copy-edited version of the reference list submitted by the author. Reference lists for the 2011 SEG Technical Program Expanded Abstracts have been copy edited so that references provided with the online metadata for each paper will achieve a high degree of linking to cited sources that appear on the Web.

REFERENCES

Grossmann, A., and J. Morlet, 1984, Decomposition of Hardy functions into square integrable wavelets of constant shape: SIAM Journal on Mathematical Analysis, **15**, no. 4, 723–736, doi:10.1137/0515056.

Huang, J., L. Gao, and Y. Gao, 2007, Side lobes of wavelets impact identification of thin sand bodies: Applied Geophysics, **4,** no. 2, 111–117.

Lichman, E., 2003, Unified approach to gas and fluid detection on instantaneous seismic wavelets: 73rd Annual International Meeting, SEG, Expanded Abstracts, 1699–1702.

Ricker, N., 1940, The form and nature of seismic waves and the structure of seismograms: Geophysics, **5**, 348–366, doi:10.1190/1.1441816.

Taner, M. T., F. Koehler, and R. E. Sheriff, 1979, Complex seismic trace analysis: Geophysics, **44**, 1041–1063, doi:10.1190/1.1440994.

Teolis, A., 1998, Computational signal processing with wavelets: Birkhaüser. http://www.mathworks.cn/access/helpdesk/help/toolbox/wavelet/ch06_ad9.html.

Widess, M. B., 1973, How thin is a thin bed?: Geophysics, **38**, no. 6, 1176–1180, doi:10.1190/1.1440403.